Spectrochimica Acta Part A 79 (2011) 236–244

Contents lists available at ScienceDirect

Spectrochimica Acta Part A: Molecular and Biomolecular Spectroscopy

journal homepage: www.elsevier.com/locate/saa

Fluorescence resonance energy transfer from a bio-active imidazole derivative 2-(1-phenyl-1H-imidazo[4,5-f][1,10]phenanthrolin-2-yl)phenol to a bioactive indoloquinolizine system

Jayaraman Jayabharathi*, Venugopal Thanikachalam, Marimuthu Venkatesh Perumal, Natesan Srinivasan

Department of Chemistry, Annamalai University, Annamalainagar, Tamilnadu 608002, India

ARTICLE INFO

Article history:
Received 4 January 2011
Received in revised form 18 February 2011
Accepted 25 February 2011

Keywords:
Chemisensor
FRET
Forester distance
Stern–Volmer plot
Lippert–Mataga plot
DFT

ABSTRACT

Novel donor imidazole derivative, 2-(1-phenyl-1H-imidazo [4,5-f][1,10]phenanthrolin-2-yl)-phenol (PIPP) was screened as highly sensitive chemisensor for transition metal ions and it can be used as a "multi-way" optically switchable material. Solvatochromic effects on the fluorescence behaviour of PIPP were studied in different solvents. The fluorescence of PIPP was highly sensitive to both the polarity as well as protic nature of the solvent. Fluorescence (Forster) resonance energy transfer (FRET) process from PIPP to a potent bioactive indoloquinolizine molecule was studied and it is argued that long-range dipole–dipole interaction is operating for the energy transfer mechanism. The energy transfer efficiency (E) and the distance between the acceptor and the donor (r_0) have been determined.

1. Introduction

Recently, heterocyclic imidazole derivatives have attracted considerable attention because of their unique optical properties [1] and used for preparing functionalized materials [2]. Imidazole nucleus forms the main structure of human organisms, i.e., the amino acid histidine, Vitamin B_{12}, a component of DNA base structure and also has significant analytical applications utilizing their fluorescene and chemiluminescence properties [3].

The present article deals with the solvent dependent fluorescence behaviour of a newly designed imidazole derivative, 2-(1-phenyl-1H-imidazo[4,5-f][1,10]phenanthrolin-2-yl)-phenol (PIPP) due to the presence of phenanthroline function and it behaves as a Lewis base due to the presence of the two diiminic nitrogen atoms. We have also exploited the fluorescence resonance energy transfer (FRET) from PIPP to the bioactive nitrogen heterocycle namely 3-acetyl-4-oxo-6,7-dihydro-12H-indolo-[2,3-a]quinolizine (AODIQ) [4]. The indole nucleus appears to be a promising basis for the design and synthesis of new derivatives that can effectively protect the nervous system [5]. Carbazoles and β-carbolines containing the indole nucleus are now well established as potent bioactive molecules. β-Carbolines are known to be efficient cancer cell photosensitizers and are used in photodynamic therapy (PDT). Since FRET causes a number of important biological phenomena, much interest lies in FRET studies between two potent bioactive molecules in vitro. Given the broad-range biological activities of imidazoles and indoloquinolizines, we became interested in the FRET studies between PIPP and AODIQ. The present FRET study has been performed considering its future application in PDT.

An important property that makes imidazole derivatives more attractive as a chelator is the appreciable change in its fluorescence upon metal binding. Therefore, imidazole derivatives have been used to construct highly sensitive fluorescent chemisensors for sensing and imaging of metal ions and its chelates in particular those with Ir^{3+} are major components for organic light emitting diodes [1] and are promising candidates for fluorescent chemisensors for metal ions. In continuation of our recent research experimental results [6–15], in the present paper we summarized a comprehensive study of the imidazole derivative and its structure was characterized by NMR spectra. Photophysical, photochemical studies, its chemisensor behaviour and FRET studies were analyzed and discussed. Theoretical calculations were carried out by using Gaussian-03 program [16] to supplement the experimental results.

* Corresponding author. Tel.: +91 9443940735.
E-mail address: jtchalam2005@yahoo.co.in (J. Jayabharathi).

1386-1425/$ – see front matter © 2011 Elsevier B.V. All rights reserved.
doi:10.1016/j.saa.2011.02.049

2. Experimental

2.1. Materials and methods

1,10-Phenanthroline-5,6-dione (Sigma–Aldrich Ltd.), salicylaldehyde (S.D. fine.), aniline (S.D. fine) and all the other reagents used without further purification. 3-Acetyl-4-oxo-6,7-dihydro-12H indolo-[2,3-a]quinolizine (AODIQ) was synthesized in the laboratory using the method mentioned elsewhere [16]. It was purified by column chromatography and the purity of the compound was checked by thin layer chromatography (TLC). Further, the compound was vacuum sublimed before use.

2.2. Optical measurements and composition analysis

NMR spectra were recorded for PIPP on a Bruker 500 MHz. The ultraviolet–visible (UV–vis) spectra were measured on UV–Vis spectrophotometer (Perkin Elmer, Lambda 35) and corrected for background due to solvent absorption. Photoluminescence (PL) spectra were recorded on a (Perkin Elmer LS55) fluorescence spectrometer. MS spectra were recorded on a Varian Saturn 2200 GCMS spectrometer.

2.3. Computational details

Quantum mechanical calculations were used to carry out the optimized geometry, HOMO–LUMO energies and MEP with Gaussian-03 program using the Becke3-Lee-Yang-Parr (B3LYP) functional supplemented with the standard 6-311++G(d,p) basis set [17,18].

2.4. General procedure for the synthesis of 2-(1-phenyl-1H-imidazo[4,5-f][1,10]phenanthro-lin-2-yl)phenol (PIPP)

The experimental procedure was used as the same as described in our recent papers [6–15]. The imidazole derivative, PIPP was synthesized from an unusual four components assembling of 1,10-phenanthroline-5,6-dione, ammonium acetate, aniline and salicylaldehyde (Scheme 1).

2.5. 2-(1-Phenyl-1H-imidazo[4,5-f][1,10]phenanthro-lin-2-yl)phenol (PIPP)

Yield: 55%. mp = 289 °C, Anal. calcd. for $C_{25}H_{16}N_4O$: C, 77.3; H, 4.15; N, 14.42. Found: C, 76.65; H, 4.08; N, 13.98. ^{1}H NMR (500 MHz, $CDCl_3$): δ 4.90 (S, 1H), 6.63 (d, 1H), 6.81 (m, 2H), 7.01–7.16 (m, 1H), 7.29 (d, 2H) [*o*-hydroxy phenyl ring], 7.59–7.75 (Aromatic protons of aniline ring), 9.04 (d, 2H, H-aryl, J = 4.5 Hz), 9.10 (d, 2H, J = 8.0 Hz), 9.20 (d, 2H, J = 5.6 Hz). ^{13}C (100 MHz, $CDCl_3$): δ 115.86, 119.42, 121.50, 121.85, 122.40, 122.91, 127.53, 127.61, 128.30, 129.05, 129.72, 130.67, 135.20, 136.40, 137.40, 149.4, 150.00, 154.1, 156.02. MS: m/z 388.13,calcd 388.42.

3. Results and discussion

3.1. Photo physical properties of imidazole derivative (PIPP) in solution

Absorption and emission properties of the imidazole derivative, PIPP have been studied in various solvents. The absorption band maxima (λ_{abs}), emission band maxima (λ_{emi}) and the associated stokes shift (ΔE) are shown in Table 1.

The imidazole derivative (PIPP) fluoresces strongly in solution at room temperature. The luminescence excitations spectra of PIPP are in coincide with their absorption spectra and differ from their emission spectra. Therefore, the fluorescence of the imidazole derivative was taken for discussion.

3.2. Effect of solvent on the absorption spectra

The shift of absorption with different solvents observed for PIPP is shown in Fig. 1. The shift can be described as hypsocromic or bathochromic depending on whether the absorption maximum occurs at a lower or higher wavelength respectively (Table 1). In the present study, the absorption spectra shifts to higher wavelength with increasing solvent polarity, indicating a bathochromic shift. Normally, the bathochromic shift happens when the dipole moment of the compound increases during the electronic transition i.e., the ground state dipole moment is lesser than the excited state dipole moment ($\mu_g < \mu_e$) and the excited state is formed in solvent cage of already partly oriented solvent molecules [19,20].

Thus more polar solvents favour the stabilisation of excitation of the imidazole derivative. By examination of the structure of imidazole derivative, the electrons are expected to delocalise between the nitrogen atoms. In addition hydrogen bonding between the solvent and nitrogen atom of the imidazole may induce electron

Table 1
Photophysical properties of the imidazole derivative PIPP.

Solvents	λ_{abs} (nm)	λ_{emi} (nm)	Stokes shift (cm^{-1})
Hexane	276	392	10,722
1,4-Dioxane	290	427	11,064
Benzene	286	429.5	11,682
Chloroform	287	430.5	11,587
Ethyl acetate	285	431.0	11,886
Dichloromethane	292	436.0	11,311
1-Butanol	290	438.0	11,652
Ethanol	289	440.0	11,875
Methanol	288	441.5	12,072
Acetonitrile	293	442.0	11,505

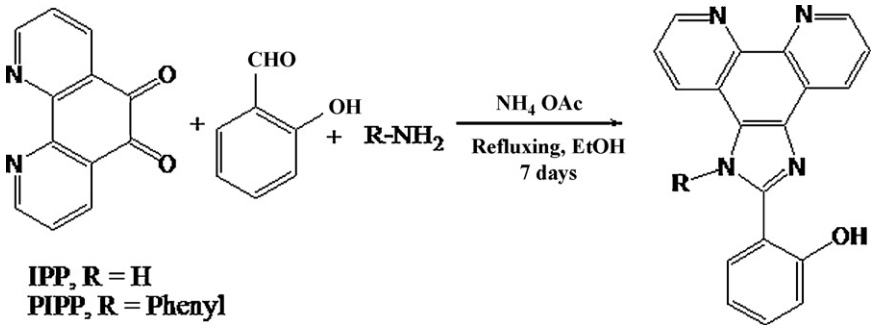

Scheme 1. Synthesis route for IPP and PIPP.

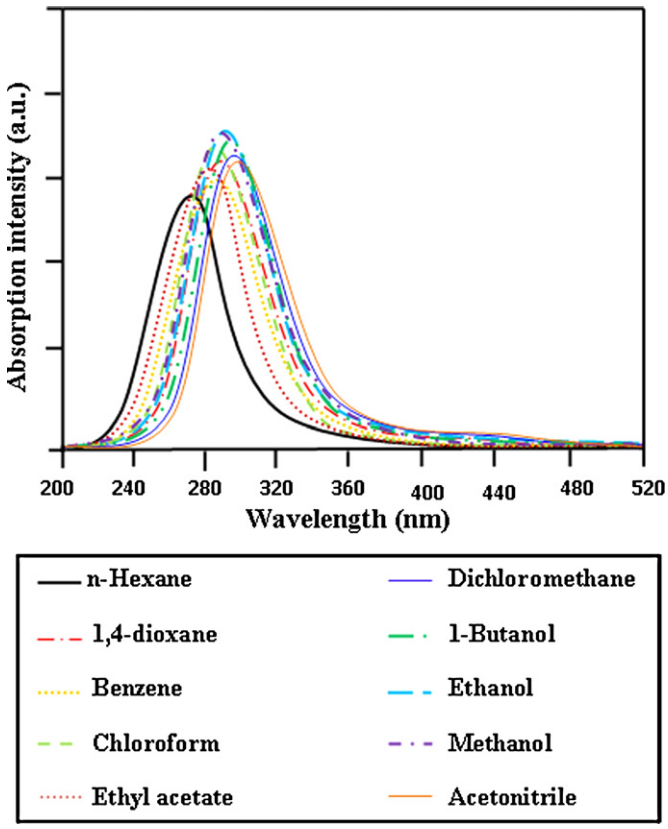

Fig. 1. Absorption solvatochromism of PIPP in various solvents.

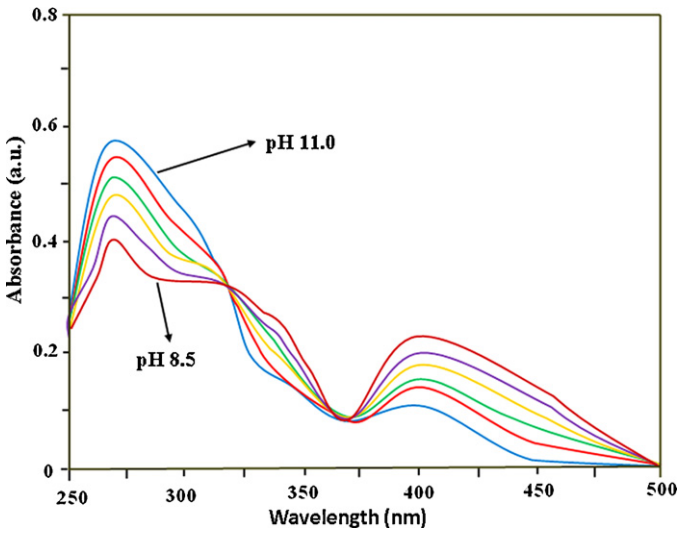

Fig. 2. Schematic representation of halochromism.

distributions. This might be the reason in protic solvents with strong hydrogen bond ability shifts to higher wavelength, but it remains fixed at lower wavelength in hexane where the formation of hydrogen bond is prevented.

Measurement of absorption solvatochromism have been interpreted with Marcus and Reichardt–Dimroth solvent functions to estimate the transition dipoles associated with low lying excited state. The linear correlation (Fig. S1) of solvent shifts of absorption band position of PIPP with Reichardt–Dimroth solvent E_T parameters is indicative of the fact that the dielectric solute solvent interactions are responsible for the observed solvatochromic shift for the imidazole derivative. The observed linear correlation (Fig. S2) of solvent shift of absorption band positions of PIPP with Marcus [21] optical dielectric solvent function $[(1 - D_{op})/(2D_{op} + 1)]$ reveal that transition dipoles associated with absorption and the direction of excited dipole is opposite to that of the ground state-dipole.

3.3. Halochromisim of the imidazole derivative PIPP

We have measured the absorption spectra of imidazole derivative (PIPP) in aprotic solvent at different pH value (Fig. 2) and it was found that the imidazole compound show halochromic behaviour dependent on the pH. In the present study, for the comparison purpose, the halochromic behaviour of 2-(1H-imidazo[4,5-f][1,10]phenanthrolin-2-yl)phenol IPP was also studied. The absorption band of IPP was red shifted with increasing pH and the absorption peak (λ_{max}) was located at 270 and 402 nm i.e., as the pH of the solution increases, the absorption band disappeared and new absorption band appeared at 402 nm. There are two isobestic points observed approximately at 320 and 370 nm which may be due to the two deprotonation steps shown in Scheme 2. The first deprotonation step of IPP around pH 8.5 is attributed to the loss of phenolic proton forming $[IPP\text{-}H]^-$ and the second deprotonation step occurs at pH 11.0 is attributed to the formation of doubly deprotonated compound $[IPP\text{-}2H]^{2-}$. The pH effect of PIPP reveal that the deprotonation step of PIPP is almost identical to the first deprotonation step of IPP, supporting our assumption that the deprotonation step of phenolic proton takes place at lower basic pH 8.5 [7].

3.4. Effect of solvent on the fluorescence spectra

Fluorescence spectral studies of PIPP were carried out in different solvents (Fig. 3), the peak maximum shifts to the right (bathochromic shift) as the solvent polarity increases (hexane to methanol). The position of the peak maximum (λ_{emi}) was plotted against the solvent dielectric constant (ε) and the observed linear correlation (Fig. S3) reveal that with increasing solvent polarity, the λ_{max} also increases. To better understand the solvent polarity effect, Lippert–Mataga relation (Fig. S4) was applied. This relation has been widely used to correlate the energy difference between the absorption maximum and the emission maximum (stokes shift) (Table 1) with solvent polarity represented by Δ_f. Stokes shift linearly increases with Δ_f implies that specific solute–solvent interactions are involved, which is known to consist of several effects i.e., dipole–dipole interactions, hydrogen bonding and dipole induced dipole interactions. Relative contribution of individual effect depends on the type of solvent used. In protic-hydrogen bonding solvents, the molecule can be stabilized through hydrogen bonding with the more electronegative nitrogen atom (N22 of the imidazole derivative). The more electronegative nature of N22 is confirmed by molecular electrostatic potential (MEP) study which is discussed in the next section. In aprotic solvents, dipole–dipole and dipole-induced dipole forces are assumed to be the predominant interactions. Decrease in total dipole moment of the solvent molecules (non-polar solvents) will result in the change of the molecular charge distributions of the imidazole derivative, PIPP. Upon excitation, molecular charge distribution is changed having less polar structure, as a result the extent of the specific hydrogen bonding might decrease [22].

3.5. Quantum yield, emission kinetics and thermodynamic properties of PIPP

The fluorescence quantum yield for PIPP (Table 2) were measured in acetonitrile, using coumarin 47 in ethanol as a standard

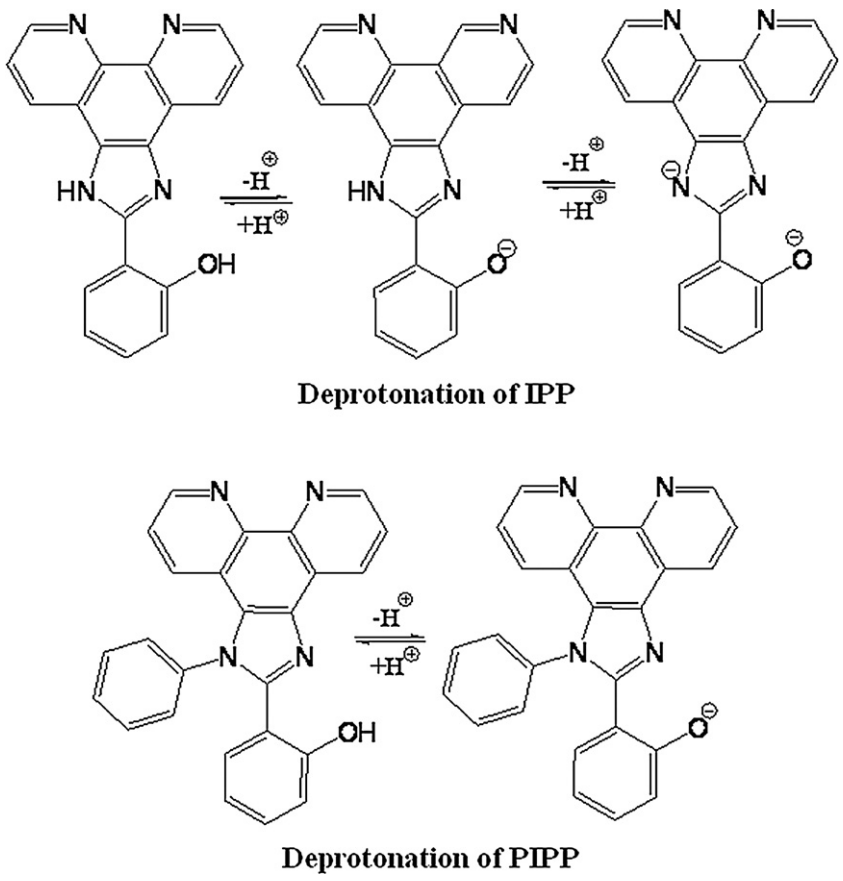

Scheme 2. Deprotonation steps of IPP and PIPP.

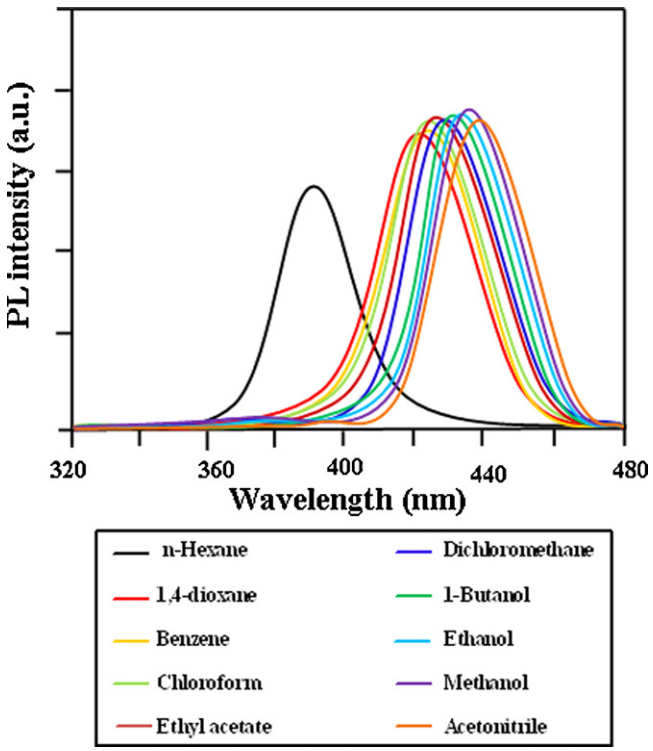

Fig. 3. Emission solvatochromism of PIPP in various solvents.

according to the equation,

$$\Phi_{unk} = \Phi_{std}\left(\frac{I_{unk}}{I_{std}}\right)\left(\frac{A_{std}}{A_{unk}}\right)\left(\frac{\eta_{unk}}{\eta_{std}}\right)^2 \quad (1)$$

where Φ_{unk}, Φ_{std}, I_{unk}, I_{std}, A_{unk}, Φ_{unk} and Φ_{std} are the fluorescent quantum yields, the integration of the emission intensities, the absorbances at the excitation wavelength and the refractive indexes of the corresponding solution for the sample and the standard, respectively. The radiative and non-radiative decay was calculated by these equations $k_r = \Phi_p/\tau$, $k_{nr} = 1/\tau - \Phi_p/\tau$, $\tau = (k_r + k_{nr})^{-1}$, where k_r, k_{nr} are the radiative and non-radiative deactivation, τ_f is the life time of the S_1 excited state.

3.6. HOMO–LUMO energies of imidazole derivative PIPP by DFT method

The frontier orbitals (HOMO and LUMO) determined the way in which the molecule interacts with other species. The frontier orbital gap (Table 2) helps to characterize the chemical reactivity and kinetic stability of the molecule. A molecule with a small frontier orbital gap is more polarizable and is generally associated with high chemical reactivity, low kinetic stability and is also termed as soft molecule [7]. The HOMO is the orbital that primarily acts as an electron donor and the LUMO is the orbital that largely acts as the electron acceptor. The 3D plots of the frontier orbitals HOMO and LUMO of PIPP is shown in Fig. S5. The HOMO is located on the imidazole ring (not on the phenanthroline ring) and the *o*-hydroxy phenyl ring attached to the C34 carbon of the imidazole ring and the LUMO located on the phenanthroline ring and not on the two phenyl rings attached to the N21 and C34 carbons of the imidazole rings). The HOMO → LUMO transition implies that intramolecular charge transfer takes place [23] within the molecule.

Table 2
Electronic properties of PIPP.

$\prod$	HOMO−1 (ev)	HOMO (ev)	LUMO (ev)	LUMO+1 (ev)	E_g ($E_{HOMO-1} - E_{LUMO}$) (ev)	E_g ($E_{HOMO} - E_{LUMO}$) (ev)
0.62	−0.25	−0.255	0.083	0.090	−0.378	−0.338

Therefore, introduction of an electron donating substituent into the phenyl ring attached to the C34 carbon raises the energy of the HOMO resulting in a red-shift of the emission. On the other hand, the introduction of the electron withdrawing substituent into the aldehydic phenyl ring lowers the energy of the HOMO, leading to the blue shift of the emission. The calculated energy gap explains the eventual charge transfer interactions within the molecule. The optimized HOMO−1, HOMO, LUMO and LUMO+1 molecular orbitals of PIPP reveal that HOMO−1 and HOMO have identical nodal patterns i.e., nodal between the C34 *o*-hydroxy phenyl ring (partly) and the imidazole ring. In the case of LUMO and LUMO+1orbitals, no nodal between the imidazole ring and the C34 *o*-hydroxy phenyl ring. Therefore the π interaction between the two rings is anti-bonding in character. From Table 2 it was concluded that the lowest energy transition ($S_0 \rightarrow S_1$) corresponds to HOMO → LUMO transition having higher oscillator strength and the higher energy transition ($S_0 \rightarrow S_2$) corresponds to (HOMO−1 → LUMO) transition having lower oscillator strength.

The energy gap (E_g) of PIPP was calculated from the HOMO and LUMO levels. The decrease in the HOMO and LUMO energy gap explains the probable charge transfer (CD) taking place inside the chromophore. The energy gap law predicts that the rate of non-radiative decay increases when the energy gap separating the ground and excited state decreases. This relation is based on the vibrational overlap between the ground state and excited state and k_{nr} is a function of Frank–Condon overlap integral. In the case of compounds having similar excited states and vibrational coupling, a simplified form of the energy gap law is obtained that predicts a linear relationship between ln(k_{nr}) and the energy gap. This correlation suggests that decay rate constant is due to the energy gap of the compound [24] and from the emission spectra, it is observed that the emission of PIPP is due to π–π* transition only.

3.7. Molecular electrostatic potential map (MEP)

In order to prove the higher electron density at the four nitrogen atoms in PIPP, we have performed DFT calculation to get the molecular electrostatic potential (MEP) for PIPP. For the consideration of the reactive behaviour of a chemical system and to investigate the molecular structure with its physiochemical property relationships [25], the three-dimensional distribution of its MEP is helpful. In MEP diagram negative regions can be regarded as nucleophilic centres, whereas regions with positive electrostatic potential are potential electrophilic sites. The molecular electrostatic potential surface (MEP) is a plot of electrostatic potential map into the iso-electron density surface simultaneously displays molecular shape, size and electrostatic potential values and has been plotted for PIPP (Fig. 4). The MEP map of PIPP clearly suggests that oxygen and nitrogen atoms represent the most negative potential region (dark red) but the nitrogen atom seems to exert comparatively small negative potential as compared to oxygen atom. The hydrogen atom attached to the six membered ring bear the maximum positive charge (blue region). The MEP clearly confirms the existence of the electrophyllic active centres characterized by red colour. The predominance of green region in the MEP surface corresponds to a potential halfway between the two extremes red and dark blue colour.

The charge distribution of PIPP was calculated by the NBO and Mulliken methods (Fig. 5). These two methods predict the same tendencies i.e., compared to nitrogen atoms N21 and N22, oxygen atom O45 is more basic. Among the nitrogen atoms N21 and N22, N22 is considered as more basic site [26]. The charge distribution shows that the more negative charge is concentrated on oxygen atom whereas the partial positive charge resides at hydrogens.

3.8. Chemosensor fluorescent

Stokes shift is important for a fluorescent sensor. The higher stokes shift value (11,311 cm^{-1}) supplies very low background signals and resultantly allows the usage of the material in construction of a fluorescence sensor [27]. Imidazole derivatives have been used to construct highly sensitive fluorescent chemisensors for sensing and imaging of metal ions and its chelates with Ir^{3+} are the major components for organic light emitting diodes [6,7] and are promising candidates for fluorescent chemisensor for metal ions, if their radiationless channel could be blocked by metal binding. The changes in emission spectrum of PIPP depending on different concentrations of Co^{2+} (Fig. 6a). According to these spectra, when the

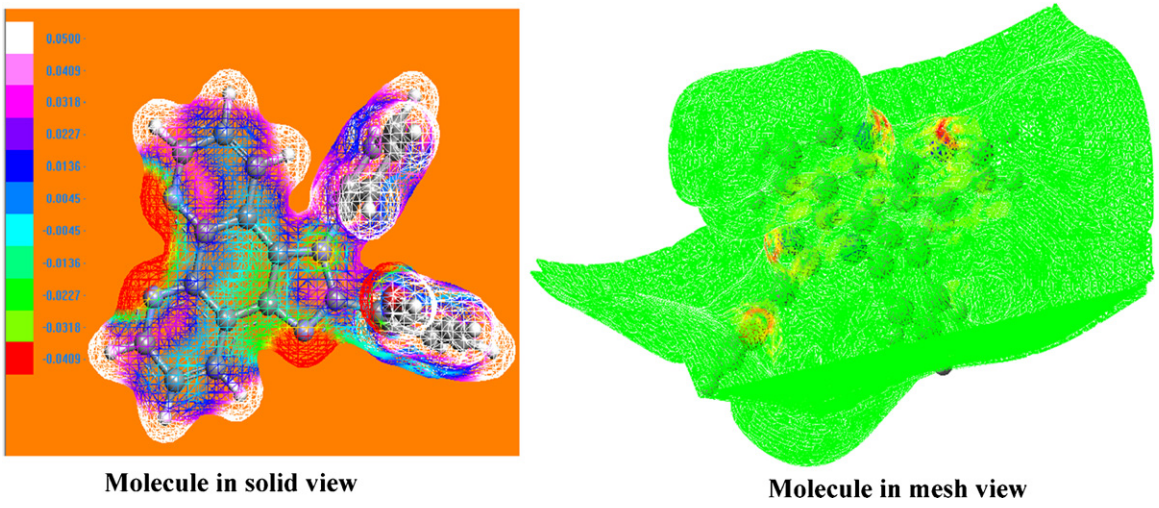

Fig. 4. Molecular electrostatic potential (MEP) diagram of PIPP.

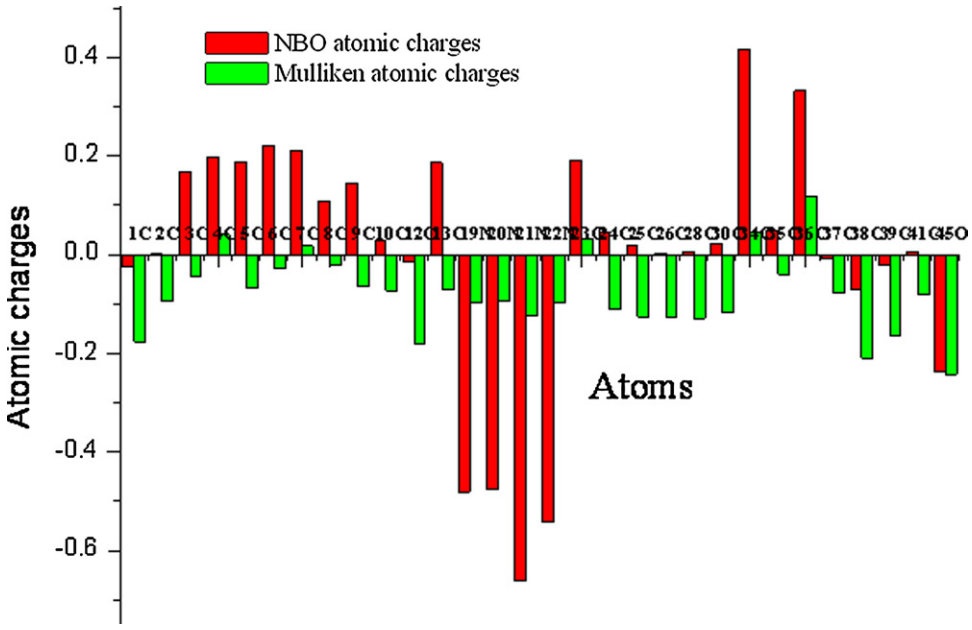

Fig. 5. Bar diagram of NBO and Mulliken atomic charges of PIPP.

concentrations of Co^{2+} are from 1×10^{-4} to 1×10^{-7} mol/L, the relative intensity changes $(I_0 - I/I_0)$ are 0.987–0.201, respectively. The quenching in fluorescence of PIPP during exposure to Co^{2+} cation indicates the complexation of PIPP with Co^{2+}. When the concentration of Co^{2+} ion increased from 1×10^{-4} to 1×10^{-7} mol/L the relative intensity changes linearly decreases. The linear regression equation is as follows.

$$\frac{I_0 - I}{I_0} = 1.150 + 0.1520 \log[Co^{2+}] \quad (2)$$

where I_0 is the emission intensity of Co^{2+} free PIPP solution and I is the emission intensity of Co^{2+} containing PIPP solution. The correlation co-efficient is 0.9907. According to the obtained results PIPP can be used as a new fluorescence sensor to detect the quantity of Co^{2+} in any sample solution depending on the relative intensity changes [28].

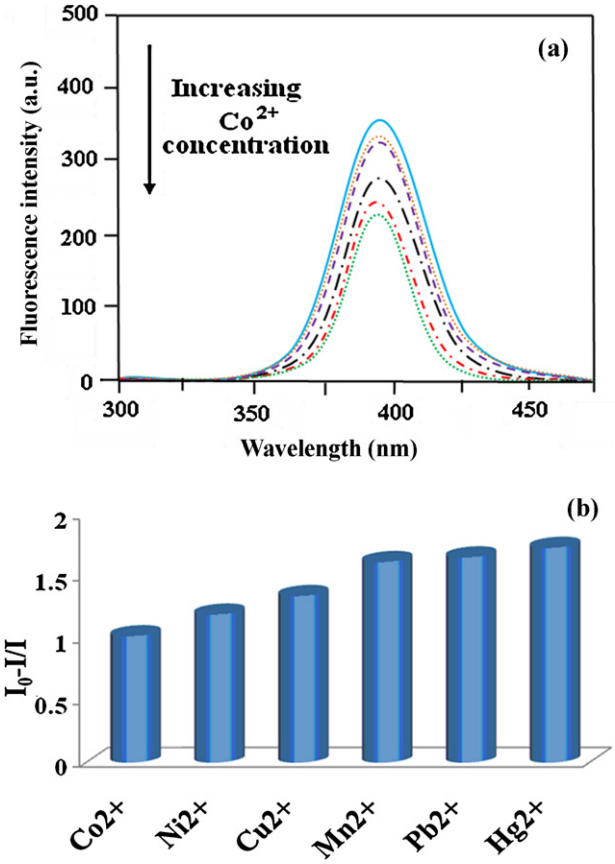

Fig. 6. (a) Fluorescent chemosensor behaviour of PIPP with Co^{2+} and (b) fluorescent chemosensor behaviour of PIPP with various metal ions.

3.9. Selective fluorescent chemosensor studies

In order to determine the selectivity of the new Co^{2+} sensor the influence of a number of transition metal cations were investigated. The experiments were performed in 1×10^{-5} mol/L of Pb^{2+}, Mn^{2+}, Ni^{2+}, Hg^{2+}, Cu^{2+} and Co^{2+}. Separate solutions of each contain 1×10^{-5} M of PIPP in 1:1 (v:v) dichloromethane/deionized water mixture. The results shows that PIPP has quite fluorescence quenching in the absence of Co^{2+} and the relative intensity changes with the tested ions of Pb^{2+}, Mn^{2+}, Ni^{2+}, Hg^{2+}, Cu^{2+} and Co^{2+} (Fig. 6b).

The selectivity results show that PIPP can be easily complex with Co^{2+} ion. Also, as seen in Fig. 11a and b, the intensity of PIPP relatively decreases in presence of some other ions such as Pb^{2+}, Mn^{2+}, Ni^{2+}, Hg^{2+}, Cu^{2+} and Co^{2+}. These decreases may be affect the quantitative measurement of Co^{2+} ion in any sample if they presence with too high concentrations. However, the known samples like sea water usually contain little concentration of these cations those are not expected to affect the quantitative measurement of Co^{2+} ion. As a result, PIPP can be used as an alternate Co^{2+} sensor by using the fluorescence technique.

3.10. Excited state dipole moment

For the determination of the difference in dipole moment of the excited state and ground state $(\Delta\mu)$, we followed the method as described by Ravi et al. [29]. According to this method, we have plotted the Stokes shift of the fluorescence maximum against E_T^N of different polar aprotic solvents (Fig. S6). From the slope of the above

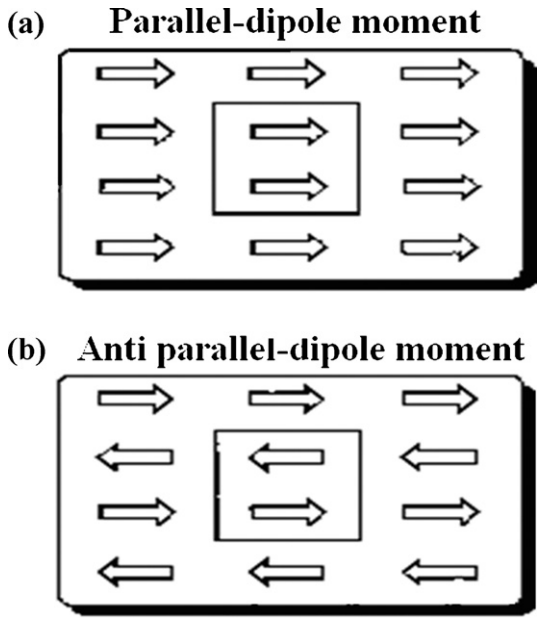

Fig. 7. Parallel and anti-parallel dipole alignments.

plot and Onsager's radius (a) for the PIPP, we have determined the $\Delta\mu$. The excited-state dipole moment has been estimated to be 15.21 D taking the value of the ground-state dipole moment as 7.92 D (corresponding to the optimized geometry of PIPP through DFT calculation).

The ratio of the difference between the absorption and fluorescence shift can be used to calculate the dipole moment of the first excited singlet state assuming that the direction of the charge transfer ($\Delta\mu$) to be in the plane of the π system. The simplified expression is $\mu_e = \mu_g$ ($\Delta E_{emi}/\Delta E_{abs}$), where μ_e and μ_g are dipole moments and ΔE_{abs} and ΔE_{emi} are the solvatochromic shifts in the absorption and fluorescence spectra in different solvents of similar refractive indices. μ_g of PIPP was calculated using the program Gaussian-03. On the basis of these values, the μ_e calculated from the above equation is 14.99 D. The calculated higher μ_e value support that the excited states of PIPP is more polar than their corresponding ground state.

The overall polarity of the synthesized imidazole derivative is small when their dipole moments aligned in a parallel fashion (Fig. 7). When the electric field is removed, the parallel alignment of the molecular dipole moment begins to deteriorate and eventually the imidazole derivative loses its NLO activity. The ultimate goal in the design of polar materials is to prepare compounds which have their molecular dipole moments aligned in the same direction.

3.11. Fluorescence (Forster's) resonance energy transfer from PIPP to AODIQ

FRET is a distance-dependent interaction between the different electronic excited states of molecules in which excitation energy is transferred from one molecule (donor) to the other (acceptor) without emission of a photon from the donor molecular system (Fig. 8). According to Forster's theory, the efficiency of FRET depends mainly on the extent of overlap between donor emission and the acceptor absorption, the orientation of the transition dipole of donor and acceptor and the distance between the donor and the acceptor [30–32]. In the present work, the origin of idea of studying the FRET from PIPP to AODIQ stemmed from the consideration of overlap of the absorption and fluorescence band positions of the two fluorophores. In dioxane solvent, PIPP absorbs appreciably at 290 nm giving fluorescence at around 430 nm. The molecule AODIQ

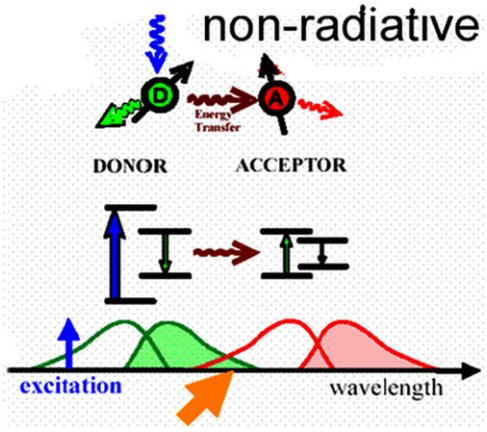

Fig. 8. FRET mechanism.

absorbs appreciably at 420 nm and emits at 455 nm [30]. Considering the fluorescence band of PIPP and the absorption band of AODIQ, this pair is an excellent pair of donor–acceptor system for the FRET study. Gradual addition of AODIQ to the PIPP solution in dioxane associated with bathochromic shift of the emission maximum along with decrease in the fluorescence intensity at 427 nm (Fig. 9) and finally a new band at 455 nm appears to correspond to the acceptor molecule. Since the emission band position of the donor (427 nm) and the acceptor (455 nm) are very close, isoemissive point is not possible, which is a main characteristic of FRET process. Absence of any additional absorption band for the mixture of PIPP and AODIQ, exploited the ground state complex of the donor–acceptor pair was not formed in the solution [33,34]. The fluorescence emission spectrum of the mixture of donor and acceptor did not show any additional new broad peak at longer wavelength confirmed the absence of exciplex formation between the excited donor and the acceptor molecules. Thus, the decrease in fluorescence intensity of the donor with increasing acceptor concentration indicates non-radiative energy transfer between the excited donor and the acceptor. Furthermore, the fluorescence excitation spectra in presence of donor and acceptor monitoring at 465 nm clearly show that an efficient Forester's type resonance energy transfer from PIPP to AODIQ system (Fig. 10).

The quenching of the fluorescence of the donor (PIPP) with the addition of acceptor (AODIQ) was followed by Stern–Volmer plot

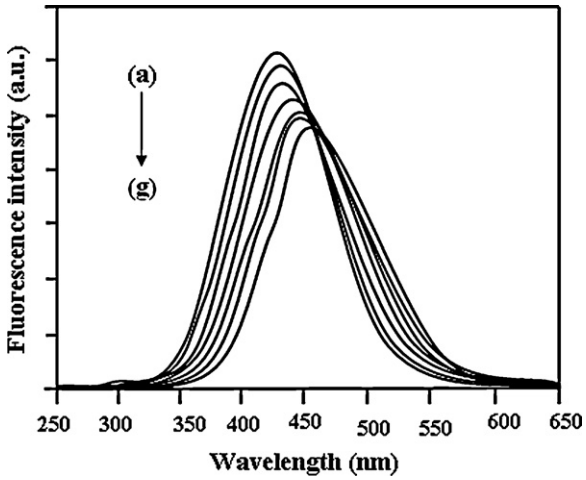

Fig. 9. Fluorescence spectra of PIPP as a function of AODIQ.

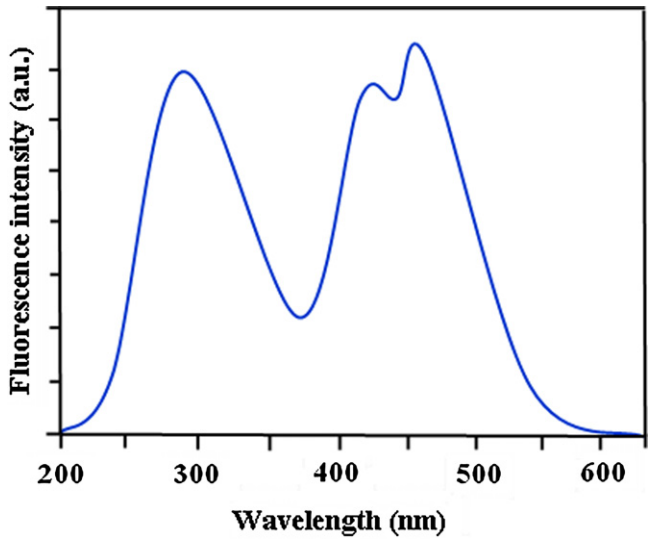

Fig. 10. Fluorescence spectra of donor and acceptor.

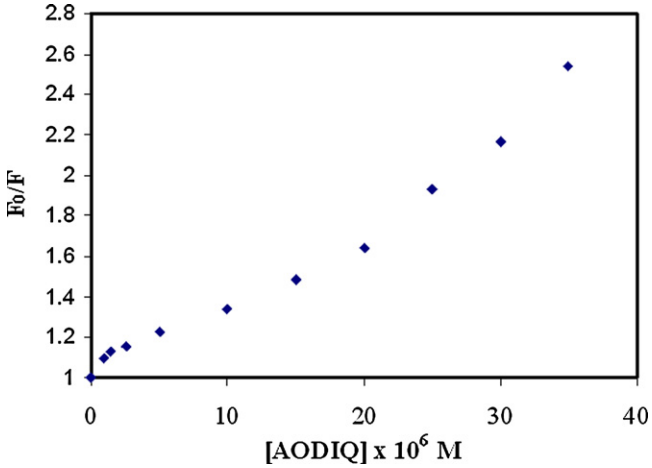

Fig. 11. Stern–Volmer plot of PIPP.

(Fig. 11).

$$\frac{F_o}{F} = 1 + k_q\tau_0[Q] = 1 + K_{SV}[Q] \quad (3)$$

From this figure, it is evident that at high concentration of acceptor it undergoes a positive deviation from the linearity. The nonlinearity was attributed to the fact that at high quencher concentration, a fraction of the fluorophore is just adjacent to the acceptor at the moment of excitation and thus immediately deactivated upon excitation. From the linear portion of the curve, we have determined the quenching rate constant (K_{SV}) value to be 3.8×10^4 ML^{-1}. This determined K_{SV} value falls in the normal range reported earlier for FRET study [33,34].

3.12. Energy transfer efficiency and distance

To understand the energy transfer efficiency between PIPP and AODIQ, we have determined the probable distance between the reacting species for the maximum energy transfer. According to the Forster non-radiative energy transfer theory [35,36], the energy transfer efficiency (E) can be calculated by the following relation:

$$E = \frac{R_0^6}{R_0^6 + r_0^6} \quad (4)$$

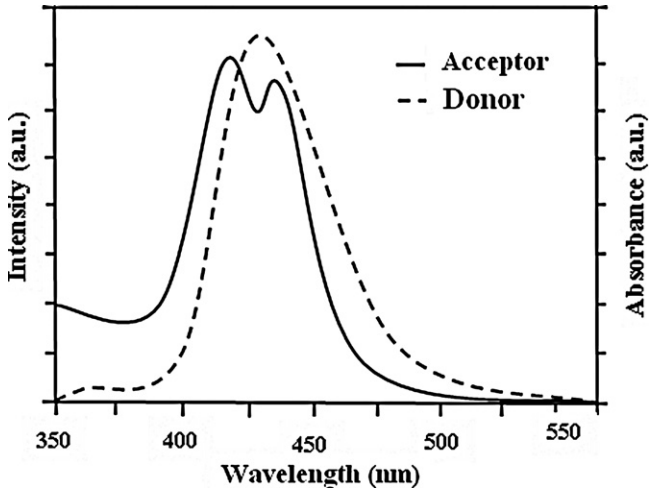

Fig. 12. Overlap of fluorescence spectrum of PIPP and absorption spectrum of AODIQ.

where r_0 is the distance between the donor and acceptor, R_0 is called the Forster's distance or critical energy transfer distance, at which the efficiency of transfer is 50% and R_0 can be calculated as follows:

$$R_0^6 = 8 : 8 \times 10^{23}[K^2 n^{-4} \Phi_D J(\lambda)] \quad \text{in} A^{6}_{0} \quad (5)$$

where k^2 is the relative orientation of the donor and acceptor molecule, n is the refractive index of the medium, Φ_D is the quantum yield of the donor in absence of the acceptor and $J(\lambda)$ is the overlap integral of the fluorescence emission spectrum of the donor and the absorption spectrum of the acceptor. The overlap spectrum ([PIPP]:[AODIQ] = 1:1) in dioxane is shown in Fig. 12. The overlap integral $J(\lambda)$ for a donor–acceptor pair is defined as

$$J(\lambda) = \int_0^\infty F_D(\lambda)\varepsilon_A(\lambda)\lambda^4 \, d\lambda \quad (6)$$

where F_D (λ) is the corrected fluorescence intensity of the donor at wavelength λ to ($\lambda + \Delta\lambda$), with the total intensity normalized to unity and ε_A (λ) is the molar extinction coefficient of the acceptor at wavelength λ. The Forster distance (R_0) has been calculated assuming random orientation of the donor and acceptor molecules. In the present case, $k^2 = 2/3$, $n = 1{:}422$, $\Phi_D = 0.62$ and with the help of the relation (5), we have calculated R_0 as 24.0 Å. The sum of collision radii of donor (PIPP) and acceptor (AODIQ) is about 12–13 Å. The significant difference between the values of the collision radii (12–14 Å) and theoretical radius of energy transfer (24.0 Å) suggest that for PIPP–AODIQ pair, long-range dipole–dipole interaction is responsible for the energy transfer mechanism consistent with the earlier proposition [33,34]. According to the Forster's non-radiative energy transfer theory, the energy transfer efficiency (E) is given by the following relation:

$$E = \frac{1 - F}{F_0} \quad (7)$$

where F is the fluorescence intensity of the donor in the presence of the acceptor and F_0 is the fluorescence intensity in the absence of the acceptor molecule. The energy transfer efficiency (E) for the pair of PIPP and AODIQ in case of 1:1 composition has been calculated and is found to be 0.29. With the knowledge of the energy transfer efficiency (E) and the critical energy transfer distance (R_0) for 1:1 composition, the distance (r_0) between the donor and acceptor molecule has been calculated to be 18 Å using relation (4). With an energy transfer efficiency 0.29 (<50%), one should expect a value of r_0 greater than the critical radius. Thus, our determined value of r_0 is rationally acceptable. The binding distance $r = 1.8$ nm is less than

8 nm which indicates that the energy transfer from PIPP to AODIQ occurs with high probability [31,32].

4. Conclusion

The present study reports the solvatochromic effect on the fluorometric behaviour of an imidazole derivative fluorophore in different solvents of varying polarity. The study reveals that fluorescence property of the molecule is very much sensitive to the polarity and the protic character of the solvent. The excited-state dipole moment has been estimated following the solvatochromic behaviour of the fluorophore with solvent polarity. Steady-state FRET from the fluorophore to a bioactive indoloquinolizine molecular system (AODIQ) has been studied in detail. K_{SV} and R_0 values suggest that a long-range dipole–dipole interaction is responsible for the energy transfer mechanism. We have developed imidazole derivative as a new set of fluorescent chemisensor for transition metal ions Hg^{2+}, Pb^{2+} and Cu^{2+} ions Co^{2+}.

Appendix A. Supplementary data

Supplementary data associated with this article can be found, in the online version, at doi:10.1016/j.saa.2011.02.049.

References

[1] W.S. Hung, J.T. Lin, C.H. Chien, Y.T. Tao, S.S. Sun, Y.S. Wen, Chem. Mater. 16 (2004) 2480–2488.
[2] K. Nakashima, Biomed. Chromatogr. 17 (2003) 83–85.
[3] A. Mallick, S.C. Bera, S. Maiti, N. Chattopadhyay, Biophys. Chem. 112 (2004) 9–14.
[4] A. Mallick, N. Chattopadhyay, Biophys. Chem. 109 (2004) 261–270.
[5] A. Mallick, B. Haldar, N. Chattopadhyay, J. Photochem. Photobiol. B 78 (2005) 215–221.
[6] J. Jayabharathi, V. Thanikachalam, K. Saravanan, N. Srinivasan, J. Fluoresc. 2010, doi:10.1007/s10895-010-0737-7.
[7] K. Saravanan, N. Srinivasan, K. Thanikachalam, J. Jayabharathi, J. Fluoresc. 2010, doi:10.1007/s10895-010-0690-5.
[8] P. Gayathri, J. Jayabharathi, N. Srinivasan, A. Thiruvalluvar, R.J. Butcher, Acta Cryst. E 66 (2010) o1703.
[9] P. Gayathri, A. Thiruvalluvar, K. Saravanan, J. Jayabharathi, R.J. Butcher, Acta Cryst. E 66 (2010) o2219.
[10] P. Gayathri, J. Jayabharathi, N. Srinivasan, A. Thiruvalluvar, R.J. Butcher, Acta Cryst. E 66 (2010) o2519.
[11] J. Jayabharathi, V. Thanikachalam, N. Srinivasan, K. Saravanan, J. Fluoresc. 2010, doi:10.1007/s10895-010-0747-5.
[12] J. Jayabharathi, V. Thanikachalam, K. Saravanan, N. Srinivasan, M. Venkatesh Perumal, Spectrochim. Acta A 2010, doi:10.1016/j.saa.2010.12.026.
[13] J. Jayabharathi, V. Thanikachalam, K. Jayamoorthy, M. Venkatesh Perumal, Spectrochim. Acta A 2010, doi:10.1016/j.saa.2010.12.027.
[14] P. Gayathri, J. Jayabharathi, N. Srinivasan, A. Thiruvalluvar, R.J. Butcher, Acta Cryst. E 66 (2010) 2826.
[15] J. Jayabharathi, V. Thanikachalam, K. Saravanan, J. Photochem. Photobiol. A: Chem. 208 (2009) 13–20.
[16] V.S. Giri, B.C. Maiti, S.C. Pakrashi, Heterocycles 22 (1984) 233–236.
[17] Guassian 03 program, Gaussian Inc., Wallingford, CT, 2004.
[18] M.J. Frisch, J.A. Pople, J.S. Binkley, J. Chem. Phys. 80 (1984) 3265–3269.
[19] D.A. Kleinman, Phys. Rev. 126 (1962) 1977–1979.
[20] C. Reichardt, Solvents and Solvent Effects in Organic Chemistry, 2nd ed., New York, 1988.
[21] A.P. Wilde, R.J. Watts, J. Phys. Chem. 95 (1991) 622–629.
[22] B. Cundalikova, L. Sikurova, Chem. Phys. 263 (2001) 415–422.
[23] K. Fukui, T. Yonezawa, H. Shingu, J. Chem. Phys. 20 (1952) 722–725.
[24] J. Brooks, Y. Babayan, S. Lamansky, P.I. Djurovich, I. Tsyba, R. Bau, M.E. Thompson, Inorg. Chem. 41 (2002) 3055–3066.
[25] M. Wagener, J. Sadowysky, J. Gasteiger, J. Am. Chem. Soc. 117 (1995) 7769–7775.
[26] P.T. Chou, D. MxMorrow, T.J. Aartsma, M. Kasha, J. Phys. Chem. 88 (1984) 4596–4599.
[27] E.L. Roberts, J. Dey, I.M. Warner, J. Phys. Chem. A 101 (1997) 5296–5301.
[28] M. Yildirim, I. Kaya, J. Fluoresc. 20 (2010) 771–777.
[29] M. Ravi, A. Samanta, T.P. Radhakrisnan, J. Phys. Chem. 98 (1994) 9133–9136.
[30] A. Mallick, S. Maiti, B. Haldar, P. Purkayastha, N. Chattopadhyay, Chem. Phys. Lett. 371 (2003) 688–693.
[31] J.R. Lakowicz, Principles of Fluorescence Spectroscopy, Plenum Press, New York, 1983 (Chapters 7 and 10).
[32] K.K. Rohatgi Mukherjee, Fundamentals of Photochemistry, Wiley Eastern, New Delhi, 1986.
[33] K.A. Kozyra, J.R. Heldt, H.A. Diehl, J. Heldt, J. Photochem. Photobiol. A: Chem. 152 (2002) 199–205.
[34] S.A. Azim, R. Ghazy, M. Shaheen, F. El-Mekawey, J. Photochem. Photobiol. A: Chem. 133 (2000) 185–188.
[35] L.A. Sklor, B.S. Hudson, R.D. Simoni, Biochemistry 16 (1977) 5100–5108.
[36] T. Forsters, Ann. Phys. 437 (1948) 55–75.